TU Delft

Delft University of Technology

# Designing thermally stimulated 1.06 mu m Nd3+ emission for the second bio-imaging window demonstrated by energy transfer from Bi3+ in La-, Gd-, Y-, and LuPO4

Lyu, Tianshuai; Dorenbos, Pieter

**DOI**
10.1016/j.cej.2019.04.125

**Publication date**
2019

**Document Version**
Accepted author manuscript

**Published in**
Chemical Engineering Journal

**Citation (APA)**
Lyu, T., & Dorenbos, P. (2019). Designing thermally stimulated 1.06 mu m Nd3+ emission for the second bio-imaging window demonstrated by energy transfer from Bi3+ in La-, Gd-, Y-, and LuPO4. *Chemical Engineering Journal*, *372*, 978-991. https://doi.org/10.1016/j.cej.2019.04.125

**Important note**
To cite this publication, please use the final published version (if applicable).
Please check the document version above.

**Copyright**
Other than for strictly personal use, it is not permitted to download, forward or distribute the text or part of it, without the consent of the author(s) and/or copyright holder(s), unless the work is under an open content license such as Creative Commons.

**Takedown policy**
Please contact us and provide details if you believe this document breaches copyrights.
We will remove access to the work immediately and investigate your claim.

*This work is downloaded from Delft University of Technology.*
*For technical reasons the number of authors shown on this cover page is limited to a maximum of 10.*

Accepted Manuscript


# Designing thermally stimulated 1.06 μm $Nd^{3+}$ emission for the second bio-imaging window demonstrated by energy transfer from $Bi^{3+}$ in La-, Gd-, Y-, and $LuPO_4$

Tianshuai Lyu, Pieter Dorenbos

PII: S1385-8947(19)30903-9
DOI: https://doi.org/10.1016/j.cej.2019.04.125
Reference: CEJ 21545

To appear in: *Chemical Engineering Journal*

Received Date: 22 February 2019
Revised Date: 2 April 2019
Accepted Date: 19 April 2019

Please cite this article as: T. Lyu, P. Dorenbos, Designing thermally stimulated 1.06 μm $Nd^{3+}$ emission for the second bio-imaging window demonstrated by energy transfer from $Bi^{3+}$ in La-, Gd-, Y-, and $LuPO_4$, *Chemical Engineering Journal* (2019), doi: https://doi.org/10.1016/j.cej.2019.04.125

This is a PDF file of an unedited manuscript that has been accepted for publication. As a service to our customers we are providing this early version of the manuscript. The manuscript will undergo copyediting, typesetting, and review of the resulting proof before it is published in its final form. Please note that during the production process errors may be discovered which could affect the content, and all legal disclaimers that apply to the journal pertain.

ACCEPTED MANUSCRIPT

# Designing thermally stimulated 1.06 μm $Nd^{3+}$ emission for the second bio-imaging window demonstrated by energy transfer from $Bi^{3+}$ in La-, Gd-, Y-, and $LuPO_4$

**Tianshuai Lyu* and Pieter Dorenbos**

Delft University of Technology, Faculty of Applied Sciences, Department of Radiation Science and Technology, section Luminescence Materials, Mekelweg 15, 2629JB Delft, The Netherlands

E-mail: T.lyu-1@tudelft.nl

## Abstract

We report a general methodology to the rational design of thermally stimulated short-wave infrared (SWIR) luminescence between ~900 and 1700 nm by a new combination of using efficient energy transfer from $Bi^{3+}$ to $Nd^{3+}$ and an adjustable hole trap depth via valence band engineering. Predictions from a vacuum referred binding energy (VRBE) diagram are combined with the data from optical spectroscopy and thermoluminescence to show the design concept by using bismuth and lanthanide doped rare earth ortho-phosphates as model examples. $Nd^{3+}$ with its characteristic $^4F_{3/2}\rightarrow{}^4I_j$ (j=9/2, 11/2, 13/2) emission in the SWIR range is first selected as the emitting centre. The energy transfer (ET) processes from $Bi^{3+}$ or $Tb^{3+}$ recombination centres to $Nd^{3+}$ are then discussed. Photoluminescence results show that the energy transfer efficiency of $Bi^{3+}\rightarrow Nd^{3+}$ appears to be much higher than of $Tb^{3+}\rightarrow Nd^{3+}$. To exploit this ET, thermally stimulated $Bi^{3+}$ A-band emission can then be designed by using $Bi^{3+}$ as a ~2.7 eV deep electron trap in $YPO_4$. By combining $Bi^{3+}$ with $Tb^{3+}$, $Pr^{3+}$, or $Bi^{3+}$ itself, the holes trapped at $Tb^{4+}$, $Pr^{4+}$, or $Bi^{4+}$ will release earlier than the electrons captured at $Bi^{2+}$.



© 2019 Manuscript version made available under CC-BY-NC-ND 4.0 license https://creativecommons.org/licenses/by-nc-nd/4.0/

ACCEPTED MANUSCRIPT

On recombination with $Bi^{2+}$, $Bi^{3+}$ in its excited state is formed generating $Bi^{3+}$ A-band emission. Due to the ET of $Bi^{3+}\rightarrow Nd^{3+}$ 1.06 μm $Nd^{3+}$ emission appears in $YPO_4$. Herein, the thermally stimulated $Nd^{3+}$ SWIR emission is achieved by hole release rather than the more commonly reported electron release. The temperature when thermally stimulated $Nd^{3+}$ SWIR emission appears can further be engineered by changing the $Tb^{3+}$ or $Pr^{3+}$ hole trap depth in $Y_{1-x}Lu_xPO_4$ by adjusting x. Such valence band engineering approach can also be applied to other compounds like $La_{1-x}Gd_xPO_4$ and $Gd_{1-x}La_xAlO_3$ solid solutions. Our work opens the avenue to motivate scientists to explore novel SWIR afterglow phosphors in a design way instead of by trial and error approach.

**Keywords:** Bismuth; valence band engineering; hole release; energy transfer; afterglow

## 1. Introduction

Afterglow is known as a self-sustained luminescence phenomenon[1-3], where a material is capable of first storing excitation energy[4], and then emitting photons for a particular time after removing the excitation source[5, 6]. This phenomenon has promising applications in various fields[7], including but not limited to information storage[8], traffic signage[9], and alternating current driven LED (AC-LED)[10]. Particularly, nanoscale infrared afterglow probes, with the advanced application in vivo bio-imaging, have attracted ever-increasing attention[11]. One of the famous examples is the $ZnGa_2O_4:Cr^{3+}$ afterglow nano-probe[12], which shows infrared emission from 650 to 750 nm.

Short-wave infrared (SWIR) light with the emission wavelength between ~900-1700 nm exhibits unique spectral properties such as reduced Rayleigh scattering, which lead to many promising applications like in anti-counterfeiting, military night-vision surveillance, and medical imaging[7, 13-16]. For instance, as compared with the near-infrared light with emission wavelength between ~700 and 900 nm, the SWIR light has higher penetration ability

ACCEPTED MANUSCRIPT

in a challenging atmosphere condition like dust, smog, fog, or rain. The SWIR range is in the second bio-imaging window, which shows promising application to arrive at super-sensitive and deep penetration medical bio-imaging. Hong *et al*. [17] reported a type of in vivo fluorescence imaging using $Ag_2S$ quantum dots with adjustable photoluminescence in the ~1100-1400 nm second near-infrared bio-imaging window. With this quantum dots based technique, however, in situ continuous 808 nm laser excitation is required during the optical imaging process, which not only causes tissue auto-fluorescence but also inevitably induces damage to the healthy tissues[18].

Currently, short-wave infrared (SWIR) afterglow luminescence between ~900-1700 nm has attracted research interest. The "self-sustained" SWIR afterglow emission without real-time external excitation not only shows higher penetration in biological tissue compared with the infrared spectral range between ~700-900 nm, but also allows the imaging to be operated in an auto-fluorescence neglectable way[19]. This broadens the avenue to arrive at better medical bio-imaging with high signal-to-noise ratio and super imaging sensitivity[20].

Compared with the many studies on afterglow phosphors with an emission wavelength between 450 nm and 750 nm[9], there are much less studies that focus on the thermally stimulated SWIR luminescence. Properties of several typical infrared afterglow phosphors are summarized in Table 1. Only a few reports show the infrared afterglow decay in absolute radiance unit[19] like $mW.sr^{-1}.m^{-2}$ and the charge carrier trapping processes are often unclear. The proposed electron release processes and duration time as provided in Table 1 then should be regarded as indicative. It turns out that a trial and error approach appears to be often applied to discover a new SWIR afterglow phosphor, and the real nature of carrier trapping processes is usually not carefully identified such as in Table 1. There is a strong wish in the rational design of SWIR afterglow between ~900-1700 nm[7].

ACCEPTED MANUSCRIPT

Methods to derive the locations of divalent and trivalent lanthanides energy levels within the band gap of inorganic crystals have now been constructed [21, 22]. Using spectroscopic data, one can construct a so-called vacuum referred binding energy (VRBE) diagram[23]. Knowledge regarding the VRBE in defect levels, such as lanthanides, conduction band (CB), or valence band (VB), then provides a powerful tool to predict luminescence and to engineer carrier transport properties[24]. Note that the VRBE-guided method is mainly used to explore visible persistent phosphors[7] and systemic exploration of SWIR afterglow phosphors based on VRBE-guided conduction band or valence band engineering is still lacking. Particularly, to the best of our knowledge, there is no report on the design of SWIR afterglow based on hole release and tailored hole trapping depth via valence band engineering.

Table 1. Carrier trapping processes, emission, and afterglow durations for typical infrared afterglow phosphors. The symbol $\leftarrow e^-$ denotes that electrons liberate at a lower temperature than holes.

| Compound | $h^+$ | transport | $e^-$ | peak (nm) | duration (h) | ref |
|---|---|---|---|---|---|---|
| $Zn_3Ga_2Ge_2O_{10}$ | $Cr^{3+}$ | $\leftarrow e^-$ | host defect | 696 | 360 | [25] |
| $ZnGa_2O_4$ | $Cr^{3+}$ | $\leftarrow e^-$ | host defect | 687 | 5 | [9] |
| $LiGa_5O_8$ | $Cr^{3+}$ | $\leftarrow e^-$ | host defect | 716 | 1000 | [26] |
| $Zn_3Ga_2SnO_8$ | $Cr^{3+}$ | $\leftarrow e^-$ | host defect | 713 | 300 | [27] |
| $MgGeO_3$ | $Yb^{3+}$ | $\leftarrow e^-$ | host defect | 1019 | 100 | [28] |
| $Zn_3Ga_2Ge_2O_{10}$ | $Ni^{2+}$ | $\leftarrow e^-$ | host defect | 1290 | 12 | [20] |
| $SrAl_2O_4$ | $Eu^{2+}$ | $\leftarrow e^-$ | $Dy^{3+}$ | 1530 ($Er^{3+}$) | 0.2 | [29] |
| $Y_3Al_2Ga_3O_{12}$ | $Ce^{3+}$ | $\leftarrow e^-$ | $Cr^{3+}$ | 1532 ($Er^{3+}$) | 10 | [30] |
| $Ca_2SnO_4$ | $Yb^{3+}$ | $\leftarrow e^-$ | host defect | 1000 | 10 | [31] |
| $MgGeO_3$ | $Pr^{3+}$ | $\leftarrow e^-$ | host defect | 1085 | 120 | [32] |
| $CdSiO_3$ | $Pr^{3+}$ | $\leftarrow e^-$ | host defect | 1085 | 120 | [32] |
| $LaAlO_3$ | $Cr^{3+}$ | $\leftarrow e^-$ | $Sm^{3+}$ | 986 ($Er^{3+}$) | 1 | [19] |
| $Y_3Al_2Ga_3O_{12}$ | $Ce^{3+}$ | $\leftarrow e^-$ | $Cr^{3+}$ | 1064 ($Nd^{3+}$) | 10 | [33] |

In this work, guided by a vacuum referred binding energy (VRBE) diagram, we will demonstrate how to design thermally stimulated $Nd^{3+}$ infrared luminescence between ~900-1700 nm by a new combination of efficient energy transfer from $Bi^{3+}$ to $Nd^{3+}$ and adjustable hole trap depth via valence band engineering in the model La-, Gd-, Y-, and $LuPO_4$

ACCEPTED MANUSCRIPT

compounds. Here, the thermally stimulated $Nd^{3+}$ SWIR emission is obtained by means of hole release rather than the more commonly reported electron release.

Fig. 1 shows the VRBE diagram for $YPO_4$ with energy level locations of $Bi^{2+}$, $Bi^{3+}$, and lanthanides. Here, $Tb^{3+}$, $Pr^{3+}$, and $Bi^{3+}$ act as ~1.45 eV, ~1.41 eV, and ~1.42 eV deep hole traps and $Nd^{3+}$ as a ~0.96 eV deep electron trap as evidenced in previous experimental work[34, 35]. The $Bi^{3+}$ is predicted to act as a ~2.7 eV deep electron trap based on the VRBE diagram prediction.

Upon charging by β- or γ-ray irradiation, free charge carriers are created that can migrate via the valence band or conduction band. The electrons can be captured in a $Bi^{3+}$, or $Nd^{3+}$ electron trap centre forming $Bi^{2+}$, or $Nd^{2+}$ (arrows 1), and the holes can be captured by $Bi^{3+}$, $Tb^{3+}$, or $Pr^{3+}$ generating $Bi^{4+}$, $Tb^{4+}$, or $Pr^{4+}$ in their ground states (arrows 2) in $YPO_4$. Because the trap depth of the 2.7 eV deep $Bi^{3+}$ electron trapping centre is ~1.25 eV deeper than that of the ~1.45 eV deep hole trapping centres of $Bi^{3+}$, $Tb^{3+}$, or $Pr^{3+}$, the hole capturing centres will liberate holes (arrow 3) to combine with electrons at $Bi^{2+}$ yielding $Bi^{3+}$ A-band emission. If there is an efficient energy transfer process from $Bi^{3+}$ to $Nd^{3+}$, then thermally stimulated $Nd^{3+}$ SWIR luminescence near 1.06 μm can appear. The engineering of the hole trap depth of $Tb^{3+}$ or $Pr^{3+}$ hole trapping centres was demonstrated in $Y_{1-x}Lu_xPO_4$ solid solutions. By increasing x, the valence band (VB) energy can be tailored. The temperature when thermally stimulated $Nd^{3+}$ ~1.06 μm luminescence appears can then be engineered by adjusting the $Tb^{3+}$ or $Pr^{3+}$ hole trap depth in $Y_{1-x}Lu_xPO_4$. We will verify all the above type of expectations, and provide a general VRBE-guided route to the rational design of thermally stimulated SWIR phosphors that can be applied to other inorganic compounds like $La_{1-x}Gd_xPO_4$ and $Gd_{1-x}La_xAlO_3$ solid solutions.

ACCEPTED MANUSCRIPT

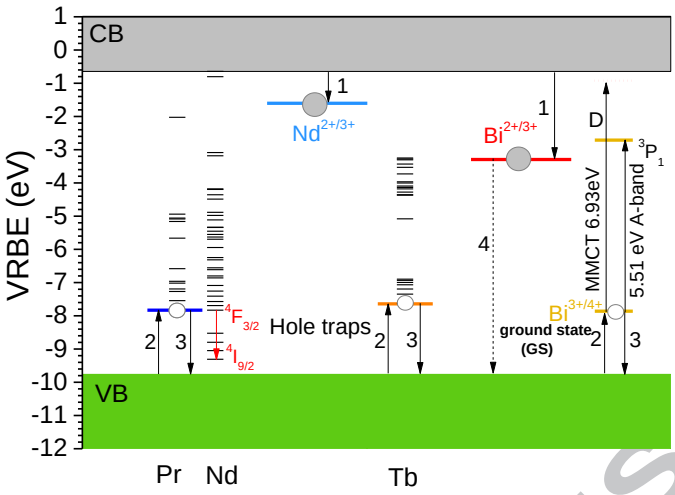


Fig. 1. Vacuum referred binding energy (VRBE) diagram of $YPO_4$ including the energy level locations for the ground states of $Nd^{2+}$, $Pr^{3+}$, $Tb^{3+}$, $Bi^{2+}$, and $Bi^{3+}$. The open circles represent holes and the filled circles are electrons. The charge carrier trapping processes indicated using numbered arrows are discussed in the text.

## 2. Experimental

All starting reagents were bought from Sigma-Aldrich and employed without further treatments. Chemical reagents $Bi_2O_3$ (99.999%), $NH_4H_2PO_4$ (99.99%), and rare earth oxides (99.999%) were utilized as starting raw materials. Samples were synthesized by high-temperature solid-state reactions. Stoichiometric mixtures were thoroughly mixed in acetone. The mixtures were fired at 400 $^oC$ for 5 h and then at 1400 $^oC$ for 10 h in a covered corundum crucible in ambient atmosphere. The heating rate for the furnace is 3 $^oC$ per minute. After cooling, the as-synthesized compounds were ground well before further measurements. Solid solutions $Y_{1-x}Lu_xPO_4$:0.005$Bi^{3+}$,0.005$Ln^{3+}$,0.005$Nd^{3+}$ ($Ln^{3+}$=Tb, and Pr) were prepared for x ranging from 0 to 1. The phase purities of all the samples were checked using a PANalytical XPert PRO x-ray diffraction system equipped with a cobalt Kα (λ=0.178901 nm) X-ray tube.

ACCEPTED MANUSCRIPT

The photoluminescence (PL) emission and excitation spectra were recorded at room temperature (RT) using a setup that consists of a UV/VIS spectrometer (Ocean Optics, QE65000), a near-infrared (NIR) spectrometer (Ocean Optics, NIRQ512), and a diode-pumped YAG: Nd laser system (NT230-100-SH/DUV-SCU). With an optical parametric oscillator (OPO), the output laser wavelength of a NT230-100-SH/DUV-SCU laser system can be tuned from 192 to 2600 nm. We used a Si-based detector QE65000 with a spectral range of 200-975 nm and an InGaAs based detector NIRQ512 with a spectral range of 900-1700 nm. The fluorescence lifetime curves were measured with a setup that includes a PerkinElmer MP-1913 photomultiplier (PMT), a UV/vis branch, a digitizer module, and an NT230-100-SH/DUV-SCU laser system. For these spectral measurements, all powder samples with different chemical composition were pressed into pills with 0.4 cm diameter and mass <20 mg.

Thermoluminescence (TL) glow curves above room temperature (300-720 K) were recorded with a setup that consists of a RISØ TL/OSL reader (model DA-15), a controller (DA-20), and an EMI9635QA photomultiplier[36]. Prior to the TL measurements, all the samples were heated to 720 K 3 times to empty all relevant traps in complete darkness under a flow of $N_2$ gas and then cooled to room temperature followed by a β irradiation charging treatment using a $^{90}Sr/^{90}Y$ β source at a dose rate of 0.7 mGy/s. For the TL recording on samples where $Bi^{3+}$ was the recombination centre, a 239 nm bandpass (239FS10-50, Andover Corporation) filter was placed between the PMT tube and the sample during the measurements.

Low-temperature thermoluminescence (LTTL) glow curves (90-450 K) were performed using a setup that consists of a $^{90}Sr/^{90}Y$ β irradiation source, a PerkinElmer channel photomultiplier tube (MP-1393), and a sample chamber that can be cooled to 90 K using liquid nitrogen under vacuum. Prior to the LTTL measurements, all the samples were heated

ACCEPTED MANUSCRIPT

to 450 K to empty all relevant traps and then charged at 90 K using β irradiation for 10 min at a dose rate of ~0.4 mGy/s. For $LaPO_4$:0.002$Bi^{3+}$,0.005$Pr^{3+}$,0.005$Nd^{3+}$ a 600 nm bandpass (600FS40-50) filter was used to select $Pr^{3+}$ emission, and for $LaPO_4$:0.002$Bi^{3+}$,0.005$Tb^{3+}$, 0.005$Nd^{3+}$, a 545 nm bandpass (545FS40-50) filter was used to monitor $Tb^{3+}$ emission.

Thermoluminescence emission spectra (TLEM) were recorded at a heating rate of 1 K/s by using the RISØ TL/OSL reader equipped with a UV/vis QE65000 spectrometer and a near infrared NIR512 spectrometer. All samples were first heated to 720 K to empty relevant traps and then charged at room temperature using γ-ray irradiation from a $^{60}$Co source. The TLEM measured by QE65000 was corrected by the wavelength dependent quantum efficiency of the QE65000 spectrometer. A correction for the TLEM recorded by the infrared NIR512 spectrometer was not made.

## 3. Results

### 3.1. Photoluminescence spectroscopy

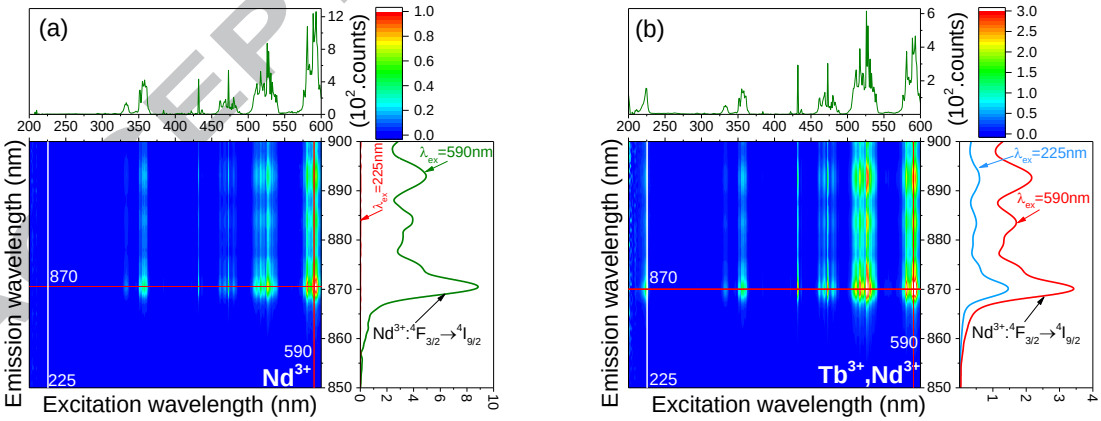

ACCEPTED MANUSCRIPT

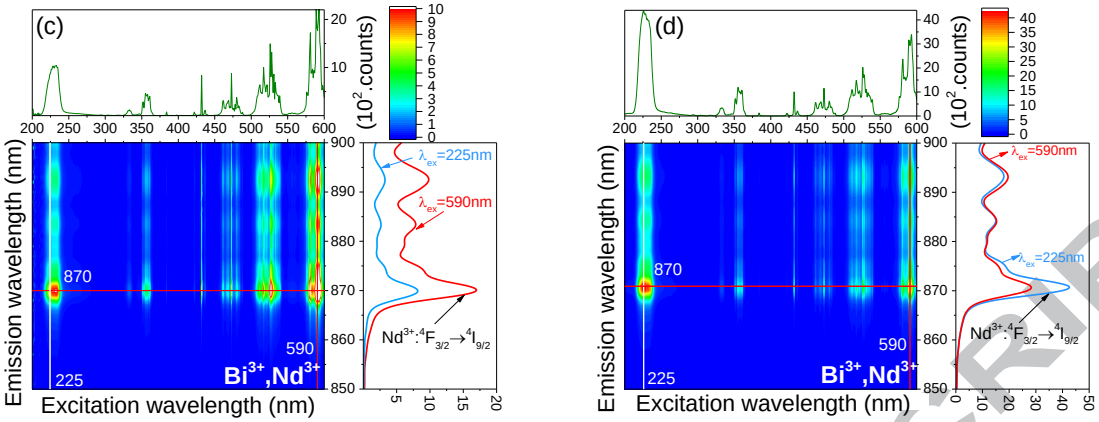


Fig. 2. Excitation-emission wavelength contour plots for (a) $YPO_4$:0.005$Nd^{3+}$, (b) $YPO_4$:0.005$Tb^{3+}$,0.005$Nd^{3+}$, (c) $YPO_4$:0.005$Bi^{3+}$,0.005$Nd^{3+}$, and (d) $YPO_4$:0.005$Bi^{3+}$, 0.02$Nd^{3+}$. The photoluminescence spectra under OPO laser excitation were recorded using a Si-based detector QE65000. A filter 10CGA-610 was used to select the $Nd^{3+}$ emission above 610 nm. All the PL spectra were corrected by both the changes of laser intensity and the wavelength dependent quantum efficiency of the QE65000 detector.

Fig. 2a)-c) shows the excitation-emission wavelength contour plots for $YPO_4$:0.005$Nd^{3+}$, $YPO_4$:0.005$Tb^{3+}$,0.005$Nd^{3+}$, and $YPO_4$:0.005$Bi^{3+}$,0.005$Nd^{3+}$. Characteristic $Nd^{3+}$ 4f-4f excitation bands between 325-600 nm appear in $YPO_4$:0.005$Nd^{3+}$ in Fig. 2a) while monitoring the 870 nm $Nd^{3+}$ $^4F_{3/2}\rightarrow{}^4I_{9/2}$ emission. A weak additional excitation band near 225 nm appears in $YPO_4$:0.005$Tb^{3+}$,0.005$Nd^{3+}$ in Fig. 2b), which is assigned to the first $Tb^{3+}$ 4f→5d spin allowed transition. The same band is observed for $Tb^{3+}$ singly doped $YPO_4$ when monitoring the $Tb^{3+}$ emission at 545 nm as shown in Fig. S1. Much stronger and broader additional excitation band near 225 nm appears in $YPO_4$:0.005$Bi^{3+}$,0.005$Nd^{3+}$ in Fig. 2c) and $YPO_4$:0.005$Bi^{3+}$,0.02$Nd^{3+}$ in Fig. 2d), which is assigned to the $Bi^{3+}$ $^1S_0\rightarrow{}^3P_1$ excitation band. The same band appears in $YPO_4$:0.005$Bi^{3+}$ in Fig. S3.

ACCEPTED MANUSCRIPT

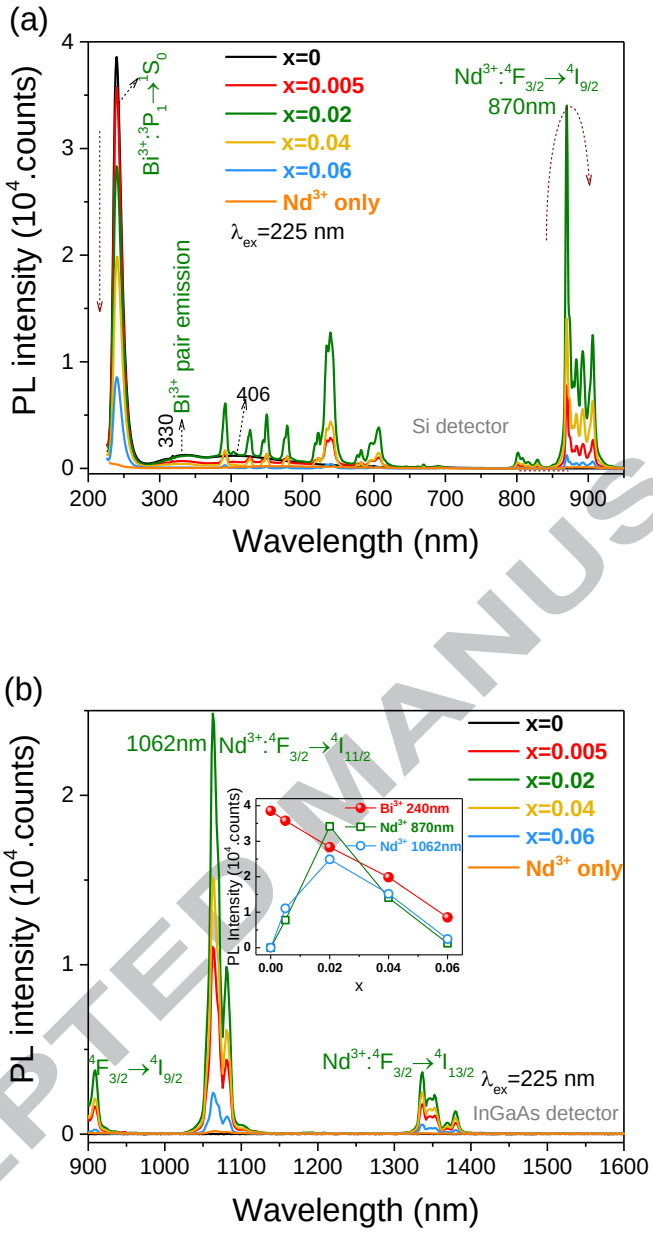


Fig. 3. 225 nm OPO laser excited photoluminescence (PL) spectra of $YPO_4$:0.005$Bi^{3+}$,x$Nd^{3+}$ (x=0-0.06) and $YPO_4$:0.005$Nd^{3+}$ crystals, a) between 225-975 nm recorded by a Si-based QE65000 detector, and b) between 900-1600 nm recorded using a InGaAs infrared detector NIRQ512. The inset in b) shows the variation of PL intensities of $Bi^{3+}$ at 240 nm, $Nd^{3+}$ at 870 and 1062 nm with increasing x.

Fig. 3 shows the photoluminescence (PL) spectra of $YPO_4$:0.005$Bi^{3+}$,x$Nd^{3+}$ (x=0-0.06) and $YPO_4$:0.005$Nd^{3+}$ between 225-1600 nm recorded by Si and InGaAs detectors upon 225

ACCEPTED MANUSCRIPT

nm excitation corresponding with the $Bi^{3+}$ A-band wavelength. Like in $YPO_4$:$Bi^{3+}$ in [37], the emission band near 240 nm is assigned to the $Bi^{3+}$ $^3P_1 \rightarrow {}^1S_0$ A-band. The broad 368-600 nm emission band peaked near 406 nm is of unknown origin. The emission band centred near 330 nm is assigned to $Bi^{4+}$-$Bi^{2+}$ pair emission[38]. With increasing x in $YPO_4$:0.005$Bi^{3+}$,x$Nd^{3+}$, the photoluminescence intensity of the $Bi^{3+}$ A-band at 240 nm continually decreases as shown in the inset of Fig. 3b), while both the PL intensities of $Nd^{3+}$ at 870 nm and at 1062 nm first increase from x=0 to x=0.02, and then decrease with further increasing x due to the concentration quenching effect of $Nd^{3+}$ emission[39].

Fig. 3 demonstrates efficient energy transfer from $Bi^{3+}$ to $Nd^{3+}$ and to further identify this energy transfer process, fluorescence decay measurements of $Bi^{3+}$ $^3P_1 \rightarrow {}^1S_0$ emission at 245 nm were carried out for the $YPO_4$:0.005$Bi^{3+}$,x$Nd^{3+}$ (x=0-0.06) samples as shown in Fig. 4a). All decay curves can be well fitted using the following single exponential formula plus a constant background intensity[40]:

$$I(t) = I_{b.g.} + I_0 \times \exp(-\frac{t}{\tau}) \quad (1)$$

Where $I_{b.g.}$ is the background intensity, $I_0$ and I(t) stand for the $Bi^{3+}$ $^3P_1 \rightarrow {}^1S_0$ emission intensities at time 0 and t, respectively. With Eq. (1) the lifetimes of the $Bi^{3+}$ $^3P_1 \rightarrow {}^1S_0$ are determined and shown in Fig. 4b). The $Bi^{3+}$ lifetime appears to decrease continually from 1.13 μs for x=0 to 0.52 μs for x=0.06 with increasing x, indicating an extra decay pathway because of a non-radiative energy transfer from the $Bi^{3+}$ $^3P_1$ level to $Nd^{3+}$.

The lifetime τ or decay rate Γ for the excited $^3P_1$ state is related to the radiative decay rate, hereafter referred to as $\Gamma_v$ ($=\tau_v^{-1}$), and the non-radiative decay rate named as $\Gamma_{nr}$ which consists of the non-radiative rates by multi-phonon relaxation ($\Gamma_{phon}$) to lower energy states and by an energy transfer process ($\Gamma_{ET}$) to $Nd^{3+}$. The following relation applies[19]

ACCEPTED MANUSCRIPT

$$\Gamma_{tot} = \Gamma_{v} + \Gamma_{phon} + \Gamma_{ET} = \tau_{Bi,Nd}^{-1} \quad (2)$$

$$\eta_{ET} = \frac{\Gamma_{ET}}{\Gamma_{v} + \Gamma_{phon} + \Gamma_{ET}} = 1 - \frac{\tau_{Bi,Nd}}{\tau_{Bi}} \quad (3)$$

where $\Gamma_{tot}$ represents the total decay rate, and $\tau_{Bi}$ and $\tau_{Bi,Nd}$ stand for the fluorescence lifetimes for the $Bi^{3+}$ $^3P_1$ level in the $Bi^{3+}$ singly and $Bi^{3+}$-$Nd^{3+}$-doped $YPO_4$. Using Eq. (3) the ET efficiencies $\eta_{ET}$ from the $Bi^{3+}$ $^3P_1$ level to $Nd^{3+}$ are estimated and shown in Fig. 4b). The $\eta_{ET}$ appears to increase with increasing x and arrives at 53.98% when x=0.06.

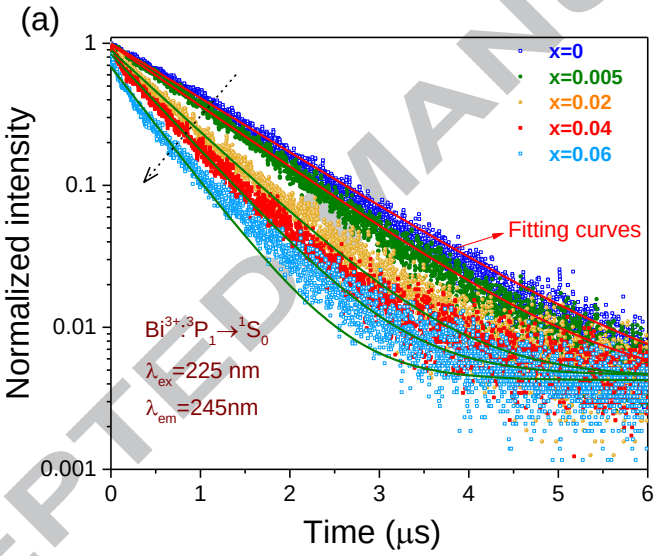

ACCEPTED MANUSCRIPT

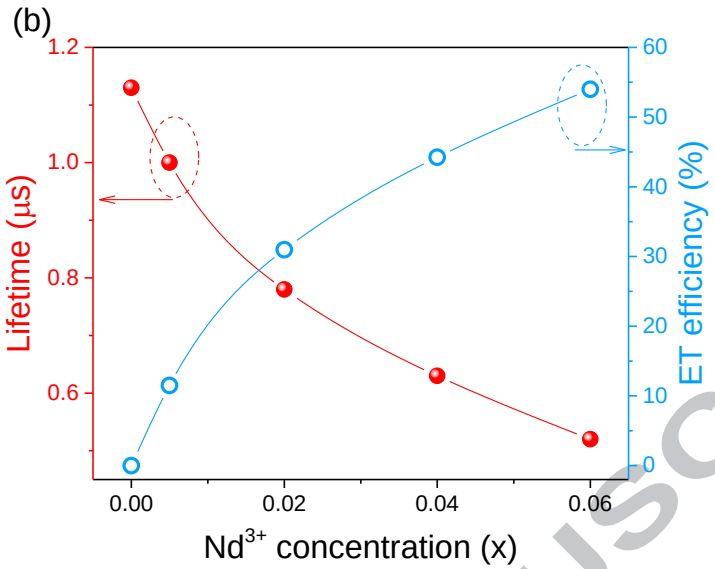


Fig. 4. (a) Fluorescence decay curves and (b) lifetime of $Bi^{3+}$ A-band emission ($^3P_1 \rightarrow {}^1S_0$) at 245 nm upon 225 nm excitation as a function of $Nd^{3+}$ concentration (x) in $YPO_4$:0.005$Bi^{3+}$, x$Nd^{3+}$ (x=0-0.06) recorded at room temperature. The $Nd^{3+}$ concentration dependence of the energy transfer efficiency of $Bi^{3+} \rightarrow Nd^{3+}$ in $YPO_4$:0.005$Bi^{3+}$,x$Nd^{3+}$ is shown.

### 3.2. Thermally stimulated luminescence

Fig. 5 presents the thermoluminescence glow curves of $YPO_4$:0.005$Bi^{3+}$,0.005$Nd^{3+}$, and $YPO_4$:0.005$Ln^{3+}$,0.005$Nd^{3+}$ (Ln=$Ce^{3+}$, and $Tb^{3+}$) after charging with β irradiation. A TL glow peak near 350 K appears in all samples where the recombination emission is either from $Bi^{3+}$ $^3P_1 \rightarrow {}^1S_0$, $Ce^{3+}$ 5d→4f, or $Tb^{3+}$ 4f→4f transitions. From the work by Bos *et al.* [41] on $YPO_4$:0.005$Ce^{3+}$,0.005$Nd^{3+}$ and $YPO_4$:0.005$Tb^{3+}$,0.005$Nd^{3+}$, this 350 K glow peak was assigned to electron release from $Nd^{2+}$ and recombination with the hole on $Ce^{4+}$ or $Tb^{4+}$. Depending on analysis methods[2, 42-45] a trapping depth E (eV) between 0.89 and 0.98 eV from this 350 K glow peak in $YPO_4$ was obtained[46] that agrees with the VRBE diagram. Compared with the experimental ~1.42 eV $Bi^{3+}$ hole trap depth found in ref. [35], the electrons trapped at $Nd^{2+}$ liberate at a lower temperature than the holes trapped at $Bi^{4+}$. They

ACCEPTED MANUSCRIPT

will recombine with the holes on $Bi^{4+}$ to give the TL glow near 350 K with typical $Bi^{3+}$ A-band emission in $YPO_4$:0.005$Bi^{3+}$,0.005$Nd^{3+}$.

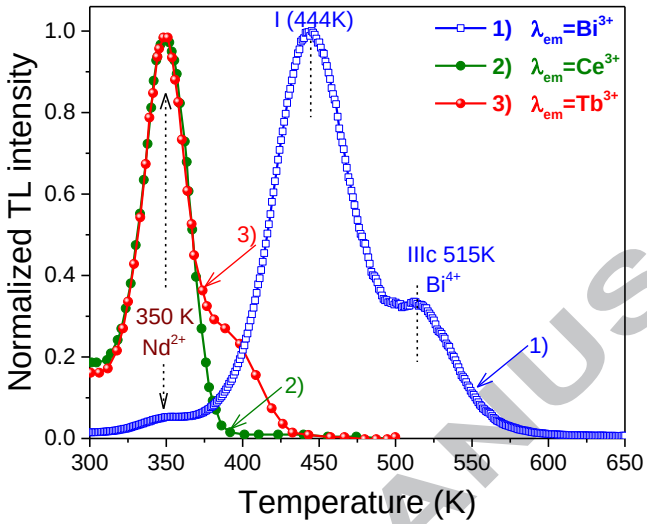


Fig. 5. Normalized TL glow curves for 1) $YPO_4$:0.005$Bi^{3+}$,0.005$Nd^{3+}$, 2) $YPO_4$:0.005$Ce^{3+}$, 0.005$Nd^{3+}$, and 3) $YPO_4$:0.005$Tb^{3+}$,0.005$Nd^{3+}$ recorded at a heating rate of 5 K/s monitoring characteristic emission either from $Bi^{3+}$, $Ce^{3+}$, or $Tb^{3+}$. The data on $YPO_4$:0.005$Ln^{3+}$,$Nd^{3+}$ (Ln=$Ce^{3+}$, and $Tb^{3+}$) crystals were derived from Bos *et al.* [41].

Thermoluminescence emission (TLEM) spectra were recorded for $YPO_4$:0.005$Nd^{3+}$, $YPO_4$:0.005$Bi^{3+}$,0.005$Nd^{3+}$, and $YPO_4$:0.005$Tb^{3+}$,0.005$Nd^{3+}$ in order to clarify the role of $Nd^{3+}$ as a 1.06 µm emitting centre during the TL readout. No TL glow peaks with typical $Nd^{3+}$ luminescence between 200-1700 nm were observed for $YPO_4$:0.005$Nd^{3+}$. Fig. 6a) shows the TL emission spectrum for $YPO_4$:0.005$Bi^{3+}$,0.005$Nd^{3+}$ recorded by a Si spectrometer. Not only characteristic $Bi^{3+}$ A-band but also $Nd^{3+}$ $^4F_{3/2}\rightarrow{}^4I_{9/2}$ emission near 870 nm appears when co-doping $Bi^{3+}$ in $YPO_4$:0.005$Nd^{3+}$. From the study in ref. [35] for $YPO_4$:0.005$Bi^{3+}$, the TL glow peaks IIIc and I that are also present in Fig. 5 were attributed to hole release from $Bi^{4+}$ and from a host-related hole trapping centre respectively. The holes recombine with the electrons captured at $Bi^{2+}$ to generate $Bi^{3+}$ A-band emission. Fig. 6b) shows the TLEM spectrum of

ACCEPTED MANUSCRIPT

$YPO_4$:0.005$Bi^{3+}$,0.005$Nd^{3+}$ recorded by an InGaAs detector in the wavelength range from 900 to 1700 nm. Thermally stimulated $Nd^{3+}$ $^4F_{3/2}\rightarrow{}^4I_{11/2}$ emission near 1.06 µm emerges. The TL glow peaks I and IIIc when monitoring the $Bi^{3+}$ A-band emission or when monitoring the $Nd^{3+}$ 4f-4f emission near 870 nm and 1.06 µm appear to have the same shape. The cut-off of black body radiation above 1650 nm in Fig. 6b) is an artefact because intensity was not corrected for the wavelength dependent quantum efficiency of the InGaAs NIR512 detector.

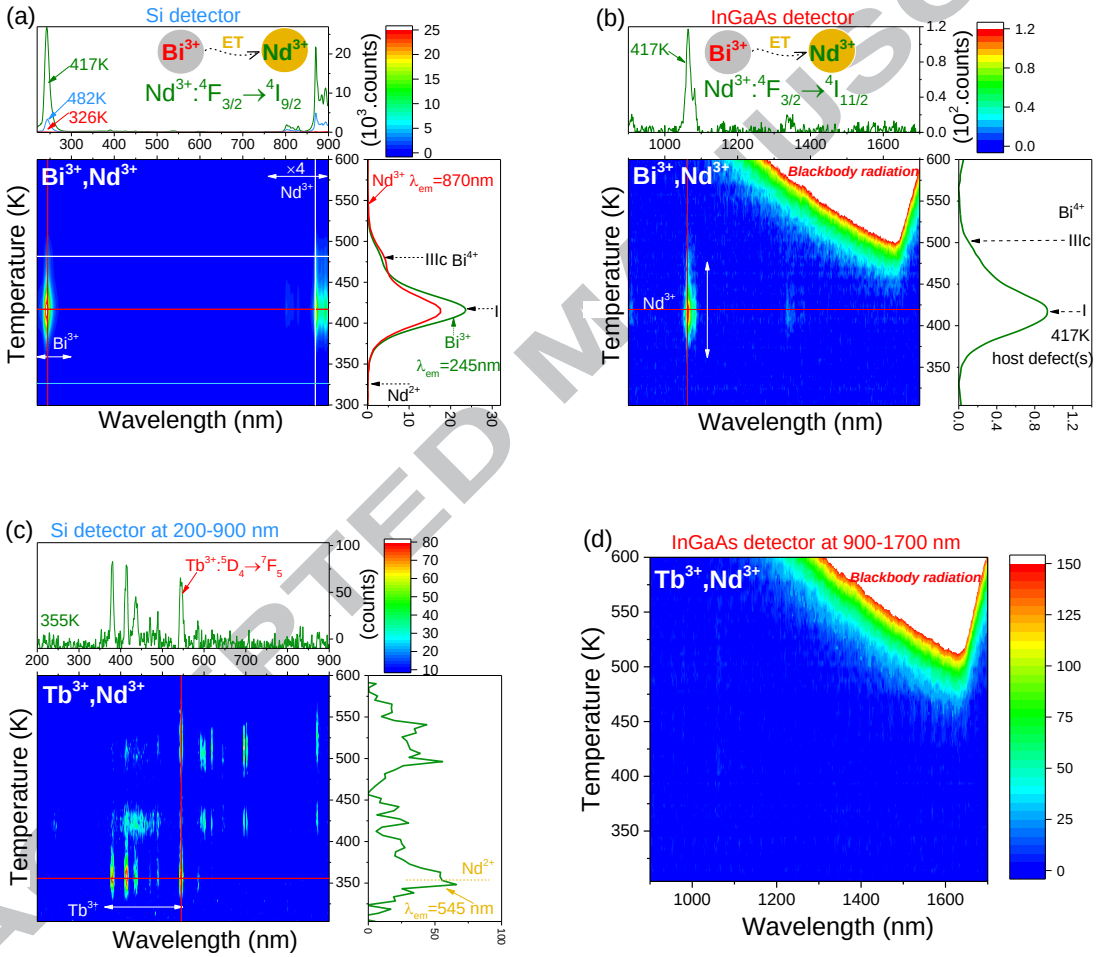


Fig. 6. Thermoluminescence emission (TLEM) plots for (a),(b) $YPO_4$:0.005$Bi^{3+}$,0.005$Nd^{3+}$ and (c),(d) $YPO_4$:0.005$Tb^{3+}$,0.005$Nd^{3+}$ recorded at a heating rate of 1 K/s after γ-ray irradiation from a $^{60}$Co source. The emission signal from each sample has been measured using a Si detector QE65000 at 200-900 nm and an InGaAs detector at 900-1700 nm.

ACCEPTED MANUSCRIPT

Fig. 6c) and d) show the TL emission spectra for $YPO_4$:0.005$Tb^{3+}$,0.005$Nd^{3+}$ in the wavelength region from 200 to 1700 nm. Characteristic $Tb^{3+}$ $^5D_4 \rightarrow {}^7F_5$ emission at 545 nm with associated TL glow band near 350 K appears in Fig. 6c), which is 300 times weaker than $Bi^{3+}$ A-band emission in $YPO_4$:0.005$Bi^{3+}$,0.005$Nd^{3+}$ in Fig. 6a). Note that the characteristic $Nd^{3+}$ 4f-4f emission near 870 nm and 1.06 μm does not appear in $YPO_4$:0.005$Tb^{3+}$,0.005$Nd^{3+}$.

Fig. 6a) shows that the $Bi^{3+}$ A-band emission of the $Bi^{4+}$ hole release glow peak IIIc is about 7 times weaker than that of the intrinsic defect hole release glow peak I in $YPO_4$:0.005$Bi^{3+}$,0.005$Nd^{3+}$. The VRBE diagram of $YPO_4$ in Fig. 1 shows that $Bi^{3+}$, $Tb^{3+}$, and $Pr^{3+}$ have almost the same ~1.42 eV hole trap depth. Their hole trapping capacity, however, may be different. We, therefore, combined $Tb^{3+}$ or $Pr^{3+}$ as a shallow hole trapping centre with $Bi^{3+}$ and $Nd^{3+}$ into $YPO_4$ to explore thermally stimulated luminescence of $Nd^{3+}$ near 1.06 μm for the second bio-imaging window. Fig. 7a) shows the TLEM spectrum for $YPO_4$:0.005$Bi^{3+}$, 0.005$Tb^{3+}$,0.005$Nd^{3+}$ after γ-ray irradiation and recorded by a Si detector in the wavelength region from 200 to 925 nm. Characteristic $Bi^{3+}$ A-band, $Tb^{3+}$ 4f-4f, and $Nd^{3+}$ $^4F_{3/2} \rightarrow {}^4I_{9/2}$ emission near 870 nm all appear. From previous study on $YPO_4$:0.005$Bi^{3+}$, 0.005$Tb^{3+}$ (Fig. S3c) in ref. [35], the TL glow peak IIIa monitoring the $Bi^{3+}$ A-band emission was attributed to hole liberation from $Tb^{4+}$ and recombination with an electron captured at $Bi^{2+}$. The simultaneous appearance of $Tb^{3+}$ 4f-4f emission was attributed to the energy transfer from $Bi^{3+}$ to $Tb^{3+}$[37]. Fig. 7b) is the TLEM plot for $YPO_4$:0.005$Bi^{3+}$,0.005$Tb^{3+}$, 0.005$Nd^{3+}$ recorded by an InGaAs spectrometer between 900-1700 nm. Thermally stimulated $Nd^{3+}$ emission near 1.06 μm appears, and the TL glow peak IIIa near 484 K when monitoring the $Bi^{3+}$ A-band emission at 245 nm, or when monitoring $Nd^{3+}$ emission at 1.06 μm or at 870 nm shares the same shape.

ACCEPTED MANUSCRIPT

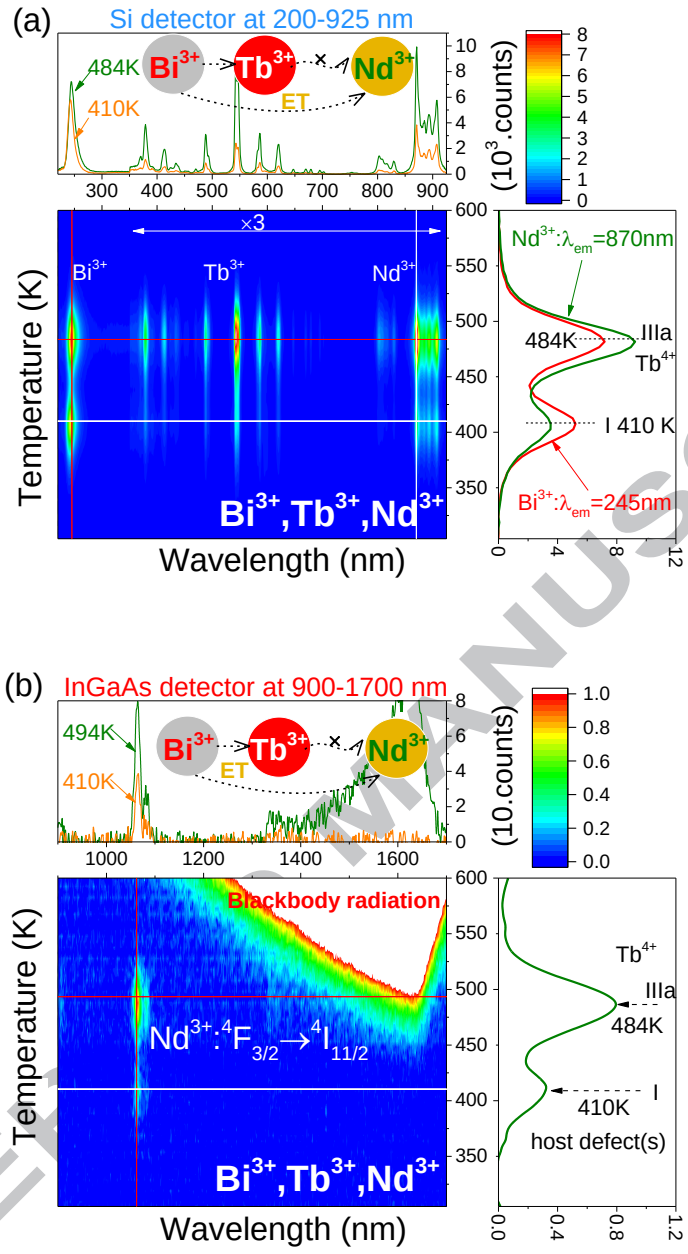


Fig. 7. TL emission (TLEM) spectra for a $YPO_4$:0.005$Bi^{3+}$,0.005$Tb^{3+}$,0.005$Nd^{3+}$ sample recorded using (a) a Si detector at 200-925 nm and (b) an InGaAs detector at 900-1700 nm at a heating rate of 1 K/s after γ-ray irradiation.

## 4. Discussion

We will first deal with the energy transfer (ET) process from $Bi^{3+}$ to $Nd^{3+}$ in $YPO_4$. Then, a new combination of that efficient energy transfer from $Bi^{3+}$ to $Nd^{3+}$ and using adjustable

ACCEPTED MANUSCRIPT

hole trap depth by valence band engineering guided by vacuum referred binding energy diagram is presented to the rational design of thermally stimulated $Nd^{3+}$ infrared emission near ~1.06 μm.

### 4.1. 1.06 μm $Nd^{3+}$ emission via energy transfer from $Bi^{3+}$ or $Tb^{3+}$

Fig. 8 shows the energy level diagram for $Bi^{3+}$, $Nd^{3+}$, and $Tb^{3+}$ in $YPO_4$. The excited $^3P_1$ state of $Bi^{3+}$ is energetically close to the $Nd^{3+}$ $^2F2_{7/2}$ and $^2F2_{5/2}$ levels, indicating that an energy transfer process from $Bi^{3+}$ to $Nd^{3+}$ is energetically possible. The excited $Nd^{3+}$ $^2F2_{7/2}$ and $^2F2_{5/2}$ levels can relax to $^4F_{3/2}$ level through non-radiative relaxation to yield $Nd^{3+}$ $^4F_{3/2}\rightarrow{}^4I_j$ (j=9/2, 11/2, and 13/2) infrared emission near 870 nm, 1062 nm, and 1337 nm respectively. This is observed in Fig. 2c) where the characteristic $Bi^{3+}$ A-band ($^1S_0\rightarrow{}^3P_1$) in the photoluminescence excitation spectrum of $Bi^{3+}$-$Nd^{3+}$-codoped $YPO_4$ appears when monitoring $Nd^{3+}$ emission. This $Bi^{3+}$ A-band increases 3 times with increasing $Nd^{3+}$ concentration in Fig. 2d), revealing that a more efficient energy transfer process from $Bi^{3+}$ to $Nd^{3+}$ occurs in $YPO_4$:$0.005Bi^{3+}$,$0.02Nd^{3+}$. The same energy transfer is demonstrated in Fig. 3 and quantified further in Fig. 4.

ACCEPTED MANUSCRIPT

ACCEPTED MANUSCRIPT

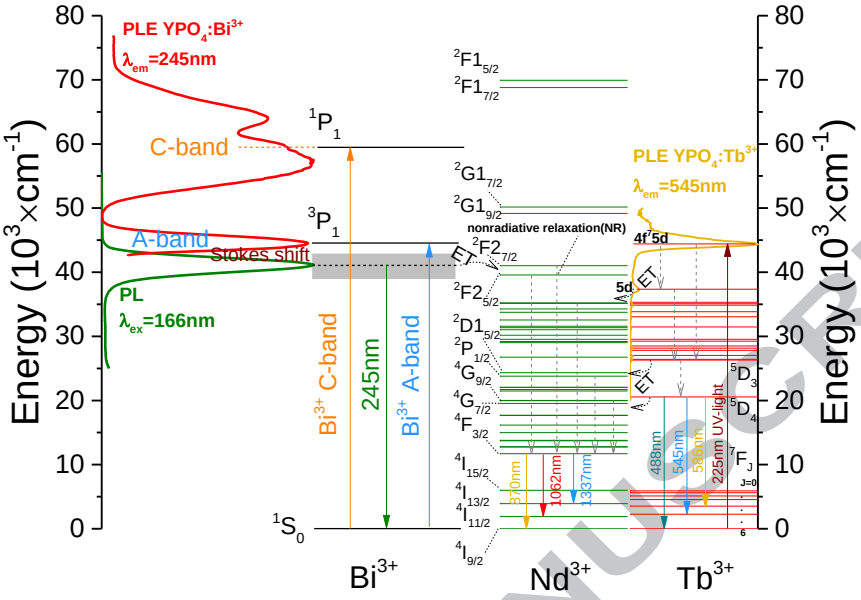


Fig. 8. Energy level diagrams of $Bi^{3+}$, $Nd^{3+}$, and $Tb^{3+}$ in $YPO_4$. The possible energy transfer routes of $Bi^{3+}$→$Nd^{3+}$ and $Tb^{3+}$→$Nd^{3+}$ are indicated. The experimental energy levels for $Nd^{3+}$ were derived from ref. [47], and for $Tb^{3+}$ 5d and $Bi^{3+}$, the levels were derived from the experimental spectroscopy in this work.

Fig. 8 also shows that the first spin allowed $Tb^{3+}$ $4f^75d$ excited state is not resonant with $Nd^{3+}$ excited states. The $Tb^{3+}$ ions in that 5d state can relax very rapidly via non-radiative relaxation to the $^5D_3$, $^5D_4$ levels or high spin [HS] $4f^75d$ near 37300 $cm^{-1}$ [48] which are energetically close to $Nd^{3+}$ levels, suggesting the possibility of energy transfer from $Tb^{3+}$ $^5D_3$, $^5D_4$ or spin-forbidden $4f^75d$ levels to $Nd^{3+}$ levels like $^4G_{7/2}$. If energy transfer from $Tb^{3+}$ to $Nd^{3+}$ is present, then a $Tb^{3+}$ 4f-5d excitation band is expected in the PL excitation spectrum of $Tb^{3+}$-$Nd^{3+}$-codoped $YPO_4$ when monitoring $Nd^{3+}$ emission. Fig. 2b) shows that a weak $Tb^{3+}$ 4f-5d excitation band near 225 nm indeed appears in $YPO_4$:0.005$Tb^{3+}$, 0.005$Nd^{3+}$ while monitoring the $Nd^{3+}$ 870 nm emission. Considering that the additional excitation band near 225 nm induced by $Tb^{3+}$ co-doping is much smaller than the one by $Bi^{3+}$ co-doping in

ACCEPTED MANUSCRIPT

$YPO_4$:0.005$Nd^{3+}$, the energy transfer efficiency of $Bi^{3+}$→$Nd^{3+}$ in $YPO_4$:0.005$Bi^{3+}$,0.005$Nd^{3+}$ appears to be much higher than that of $Tb^{3+}$→$Nd^{3+}$ in $YPO_4$:0.005$Tb^{3+}$, 0.005$Nd^{3+}$.

### 4.2. Tuneable thermally stimulated luminescence of $Nd^{3+}$ near 1.06 µm by engineering hole trap depths of $Tb^{3+}$ and $Pr^{3+}$ in $Y_{1-x}Lu_xPO_4$ and $La_{1-x}Gd_xPO_4$

Fig. 9a) shows that the vacuum referred binding energy (VRBE) in the $^2P_{1/2}$ ground state of $Bi^{2+}$ is near -3.3 eV and the VRBE in the $Bi^{3+}$ $^1S_0$, $Tb^{3+}$ and $Pr^{3+}$ $4f^n$ ground states are near -7.8 eV in the La-, Y-, and $LuPO_4$ compounds. $Bi^{3+}$ will act as an about 2.7 eV deep electron trapping centre, while $Bi^{3+}$, $Tb^{3+}$, and $Pr^{3+}$ will act as hole trapping centres which hole trap depths depend on the VRBE at the valence band top. That valence band top rises by 0.85 eV in discrete steps from Lu-, to Y-, Gd-, and to $LaPO_4$. The hole trap depths and the temperature $T_m$ for TL glow peaks due to hole release from $Tb^{4+}$, $Pr^{4+}$, or $Bi^{4+}$ should decrease accordingly. We will focus on using $Tb^{3+}$ and $Pr^{3+}$ as tuneable hole traps to demonstrate the concept of deliberate design of persistent $Nd^{3+}$ SWIR luminescence via valence band engineering.

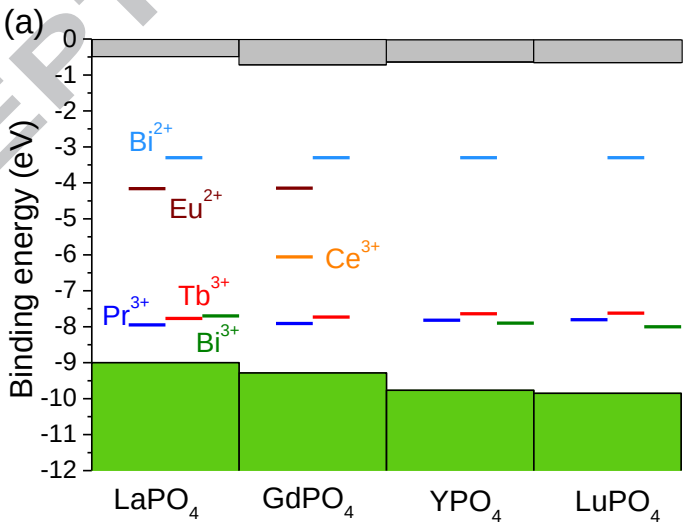

ACCEPTED MANUSCRIPT

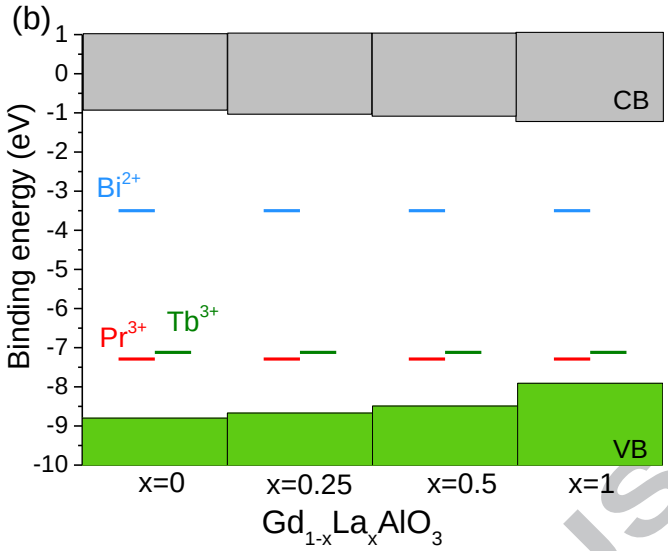


Fig. 9. Stacked VRBE diagrams for (a) $REPO_4$ and (b) $Gd_{1-x}La_xAlO_3$ solid solutions including the vacuum referred binding energy in the ground states of $Pr^{3+}$, $Tb^{3+}$, $Ce^{3+}$, $Eu^{2+}$, $Bi^{3+}$, and $Bi^{2+}$. The data on constructing the diagram (a) were obtained from ref. [34, 35]. For diagram (b) the $Tb^{3+}$ and $Pr^{3+}$ levels were obtained from ref. [49] and the $Bi^{2+}$ level near -3.5 eV for oxide compounds from ref. [50] was used.

First, we testified the adjustable thermally stimulated $Nd^{3+}$ SWIR emission in $Y_{1-x}Lu_xPO_4$ solid solutions as shown in Fig. S4-6. Although we demonstrated that the temperature of hole release can be tuned, the $T_m$ of the TL glow peaks from $Tb^{4+}$ and $Pr^{4+}$ are at a too high temperature of 500 K and shift the wrong direction. They need to be shifted close to 300 K in order to realize $Nd^{3+}$ SWIR afterglow for applications.

Fig. 9a) shows that the VRBE at the valence band top of $LaPO_4$ is about 0.85 eV higher than that in $LuPO_4$ which implies that the TL glow peaks from $Tb^{4+}$ and $Pr^{4+}$ should move towards RT. $Bi^{3+}$ and lanthanide-doped $LaPO_4$ phosphors were thus synthesized to explore $Nd^{3+}$ SWIR afterglow at room temperature. Fig. S7a) shows a TL emission plot for $LaPO_4$:0.002$Bi^{3+}$,0.005$Pr^{3+}$,0.005$Nd^{3+}$ after γ-ray irradiation. The TL glow peaks I and IIb when monitoring the $Pr^{3+}$ 4f-4f emission or when monitoring the $Nd^{3+}$ emission near 900 nm

ACCEPTED MANUSCRIPT

and 1.07 μm appear to share the same shape. Because glow peak IIb is near RT, $Nd^{3+}$ SWIR afterglow appears in $LaPO_4$:0.002$Bi^{3+}$,0.005$Pr^{3+}$, 0.005$Nd^{3+}$ in Fig. S7b).

To identify the charge carrier trapping processes, Fig. 10a) shows the low-temperature TL glow curves for $Bi^{3+}$ and lanthanides doped $LaPO_4$ by monitoring emission from $Eu^{3+}$, $Pr^{3+}$, or $Tb^{3+}$. Herein, $Bi^{3+}$ and $Eu^{3+}$ are predicted to act as ~2.81 and ~3.67 eV deep electron traps based on the VRBE diagram in Fig. 9a), while $Tb^{3+}$ and $Pr^{3+}$ act as 0.63 and 0.55 eV shallow hole trapping centres in $LaPO_4$ based on the previous experimental work in ref. [34]. By combining the deep electron trap $Eu^{3+}$ with the shallow hole trap $Tb^{3+}$ or $Pr^{3+}$, the holes trapped at $Tb^{4+}$ or $Pr^{4+}$ are liberated to recombine with the electrons at $Eu^{2+}$ producing $Eu^{3+}$ red emission[34] with TL peaks IIIa (Tb) near 240 K in Fig. 10a1) and IIIb (Pr) near 210 K in Fig. 10a3). The same glow peaks IIIa in Fig. 10a2) and IIIb in Fig. 10a4) indeed appear when $Eu^{3+}$ is replaced by the 2.81 eV deep electron trap $Bi^{3+}$. Hole release from $Tb^{4+}$ or $Pr^{4+}$ like in Fig. 10a1) or 10a3) is also present in $LaPO_4$:0.002$Bi^{3+}$,0.005$Tb^{3+}$,0.005$Nd^{3+}$ and $LaPO_4$: 0.002$Bi^{3+}$,0.005$Pr^{3+}$,0.005$Nd^{3+}$ in Fig. 10a2) and 10a4) where instead of at Eu the recombination is at Bi.

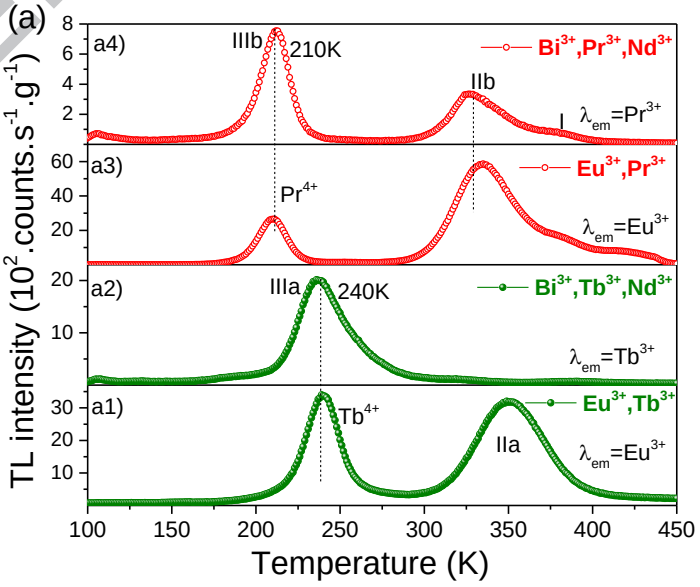

ACCEPTED MANUSCRIPT

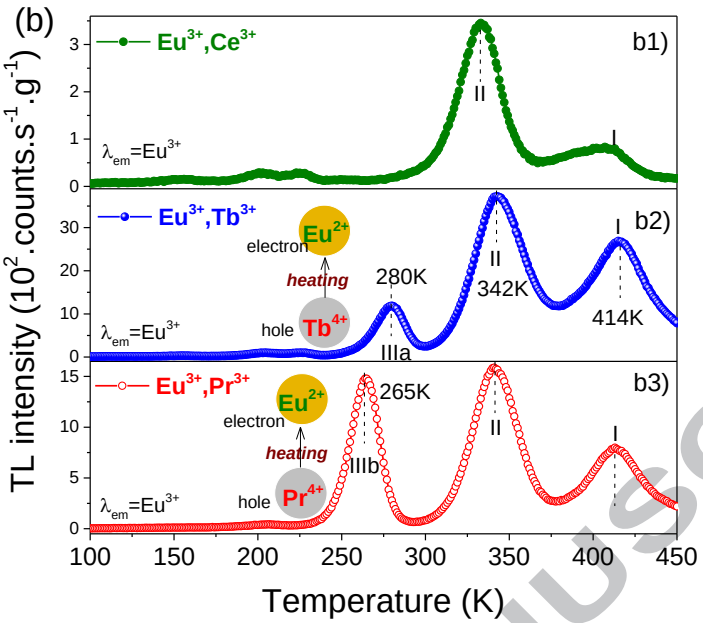


Fig. 10. Low-temperature TL glow curves for (a) $Bi^{3+}$ and $Ln^{3+}$ doped $LaPO_4$ and (b) $GdPO_4$:0.005$Eu^{3+}$,0.005$Ln^{3+}$ (Ln=Ce, Tb, and Pr) recorded at a heating rate of 1 K/s after 600s β irradiation in the temperature range between 100-450 K. $Eu^{3+}$ emission was monitored in a1)-a3) and b1-b3). The green $Tb^{3+}$ and red $Pr^{3+}$ emissions were respectively selected in a2) and a4). The TL intensities were corrected by sample mass and irradiation time.

This again demonstrates that the temperature of hole release and related SWIR emission can be engineered. However, in $LaPO_4$ the glow peaks IIIa and IIIb are shifted too far and appear below room temperature. The TL glow peaks I and IIb with red $Pr^{3+}$ emission in Fig. 10a4) cannot be attributed to electron release from host-related electron traps with recombination on $Pr^{4+}$ because the holes trapped at $Pr^{4+}$ have already disappeared as a result of recombination with the electrons at $Bi^{2+}$ near 210 K. Therefore, they are attributed to hole release from unidentified defect centres in $LaPO_4$. The appearance of $Pr^{3+}$, $Nd^{3+}$, or $Tb^{3+}$ emission in Fig. 10a4) and also Fig. S7a)-8 is assigned to energy transfer from $Bi^{3+}$, which is similar as that in $YPO_4$ in Fig. 7 and other solid solutions $Y_{1-x}Lu_xPO_4$ in Fig. S5. Supporting evidence is the appearance of the same TL glow peaks I and IIb when monitoring the

ACCEPTED MANUSCRIPT

emission either from $Pr^{3+}$ or $Nd^{3+}$ in Fig. S7a) or from $Tb^{3+}$ in Fig. S8. This is also supported by the spectral overlap of $LaPO_4$:0.002$Bi^{3+}$ at 325-600 nm emission (Fig. S10) with the 4f-4f excitation bands of $Tb^{3+}$[51], $Pr^{3+}$[52], and $Nd^{3+}$ like in Fig. 2a), which indicates the possibility of ET from $Bi^{3+}$ to $Tb^{3+}$, $Pr^{3+}$, or $Nd^{3+}$ in $LaPO_4$.

The method using $Bi^{3+}\rightarrow Nd^{3+}$ ET and engineering the hole trapping depths of $Tb^{3+}$, $Pr^{3+}$, or intrinsic hole trapping centres by valence band changing in the phosphate compounds can also be applied to solid solutions like $La_{1-x}Gd_xPO_4$ and $Gd_{1-x}La_xAlO_3$. Fig. 9a) demonstrates that the VRBE at the valence band top of $GdPO_4$ is about 0.3 eV lower than in $LaPO_4$ which indicates that the TL glow peaks IIIa near 240 K and IIIb near 210 K in Fig. 10a2) and a4) should move towards room temperature in $La_{1-x}Gd_xPO_4$ by increasing x.

To further demonstrate the design methodology of SWR afterglow phosphors in $La_{1-x}Gd_xPO_4$ solid solutions, the hole detrapping processes of $Tb^{3+}$ and $Pr^{3+}$ hole capturing centres are first studied in $GdPO_4$. Fig. 10b) shows the low-temperature TL glow curves for $GdPO_4$:0.005$Eu^{3+}$,0.005$Ln^{3+}$. Compared with $Ce^{3+}$ codoping in $GdPO_4$ in Fig. 10b1), $Tb^{3+}$ gave rise to a new TL glow peak near 280 K named as IIIa in Fig. 10b2) and $Pr^{3+}$ to a TL peak denoted as IIIb at about 15 K lower temperature in Fig. 10b3). The TL glow peak I for $GdPO_4$:0.005$Eu^{3+}$,0.005$Tb^{3+}$ was further studied by a variable heating rate plot using RISØ TL/OSL reader in Fig. S12b). This provides a frequency factor of $1.07\times10^{12}$ $s^{-1}$, which is assumed to apply to TL glow peaks IIIa and IIIb. Their trapping depths E (eV) are then determined by employing the temperature $T_m$ at the maximum of the glow curve and solving the following first-order TL-recombination kinetics formula[44, 45]:

$$\frac{\beta E}{kT_m^{\ 2}} = s\times\exp\left(-\frac{E}{kT_m}\right) \qquad (4)$$

ACCEPTED MANUSCRIPT

where β=1 K/s represents the heating rate, k denotes the Boltzmann constant ($8.62\times10^{-5}$ eV/K), and s is the frequency factor ($1.07\times10^{12}$ $s^{-1}$). With Eq. (4), the trap depths for IIIa and IIIb are respectively derived to be 0.72, and 0.68 eV.

The vacuum referred binding energy (VRBE) scheme for $GdPO_4$ in Fig. 9a) predicts that $Eu^{3+}$ and $Bi^{3+}$ act as ~3.43, and 2.78 eV deep electron traps, while $Tb^{3+}$, $Pr^{3+}$, and $Ce^{3+}$ act as 1.56, 1.38, and 3.23 eV deep hole traps. When holes are produced in the valence band, they tend to be shared between two neighbouring oxygen anions to form a thermally activated $V_k$ centre[53, 54] located above the valence band top in a VRBE scheme[34, 55]. Since La-, Gd-, $YPO_4$ are quite similar, the binding energy for a $V_k$ centre in $GdPO_4$ is assumed to be about 0.6 eV, like in La-, and $YPO_4$[34]. The effective hole trap depths of $Tb^{3+}$, $Pr^{3+}$, and $Ce^{3+}$ are then determined to be 0.96, 0.78, and 2.63 eV, respectively. Using Eq. (4) with β=1 K/s and the above predicted hole trap depths, one can estimate that the hole liberation from $Tb^{4+}$, $Pr^{4+}$, or $Ce^{4+}$ in $GdPO_4$ gives TL glow peaks $T_m$ near 369, 302, and 980 K, respectively. Obviously, the $Ce^{4+}$ hole trap is far too deep to liberate a hole between 100-450 K. The estimated TL peaks $T_m$ for hole liberation from $Tb^{4+}$ and $Pr^{4+}$ traps are in the measurement range, and we assign the TL glow peaks IIIa (0.72 eV) and IIIb (0.68 eV) to the hole liberation from $Tb^{4+}$ in Fig. 10b2) and $Pr^{4+}$ in Fig. 10b3). Considering that glow peaks I and II appear in all three samples, they are attributed hole liberation from intrinsic host defect(s) and recombination with the electrons trapped at $Eu^{2+}$.

Like $LaPO_4$ in Fig. 10a), $Bi^{3+}$ and/or $Ln^{3+}$ doped $La_{1-x}Gd_xPO_4$ solid solutions were further synthesized to explore the rational design of $Nd^{3+}$ SWIR afterglow by using adjustable hole trap depth of $Tb^{3+}$ and $Pr^{3+}$.

Fig. 11 shows the low-temperature TL glow curves for $Bi^{3+}$ and/or $Ln^{3+}$ doped $La_{1-x}Gd_xPO_4$ with x range from 0 to 1. For the samples each with the same $Pr^{3+}$ hole trap but with different

ACCEPTED MANUSCRIPT

electron trap of $Eu^{3+}$ in Fig.11a1)-a3) and of $Bi^{3+}$ in Fig. 11a4)-a6), the glow peak IIIb shares almost the same shape. It shifts from 210 K to 265 K with increasing x in $La_{1-x}Gd_xPO_4$ (also see Fig. S15), which is attributed to the increased activation energy for the hole release from the $Pr^{3+}$ hole capturing centre as a result of valence band lowering by increasing x. Similar to $Pr^{3+}$, $Tb^{3+}$ as a shallow hole capturing centre also gives a systemic shifting of TL glow peak IIIa in $La_{1-x}Gd_xPO_4$:0.002$Bi^{3+}$,0.005$Tb^{3+}$,0.005$Nd^{3+}$ in Fig. 11a7)-a11). Note that the glow peaks IIIa and IIIb become broader in the solid solutions compared with that of $LaPO_4$ and $GdPO_4$, suggesting a broader trap distribution. This indicates that the VRBE at the valence band top exhibits site-to-site fluctuations based on the statistics in $La_{1-x}Gd_xPO_4$ when La is replaced by Gd. Particularly, for x from 0.25 to 0.75 in Fig. 11a8)-a10), the broad IIIa glow peak covers the room temperature (295 K) range, which results in the $Nd^{3+}$ SWIR afterglow as shown in Fig. 12. Upon thermal stimulation at RT, the shallow $Tb^{4+}$ hole trap spontaneously liberates holes to recombine with electrons at $Bi^{2+}$, producing $Bi^{3+}$ in its excited state followed by $Nd^{3+}$ SWIR persistent luminescence as a result of energy transfer from $Bi^{3+}$.

ACCEPTED MANUSCRIPT

ACCEPTED MANUSCRIPT

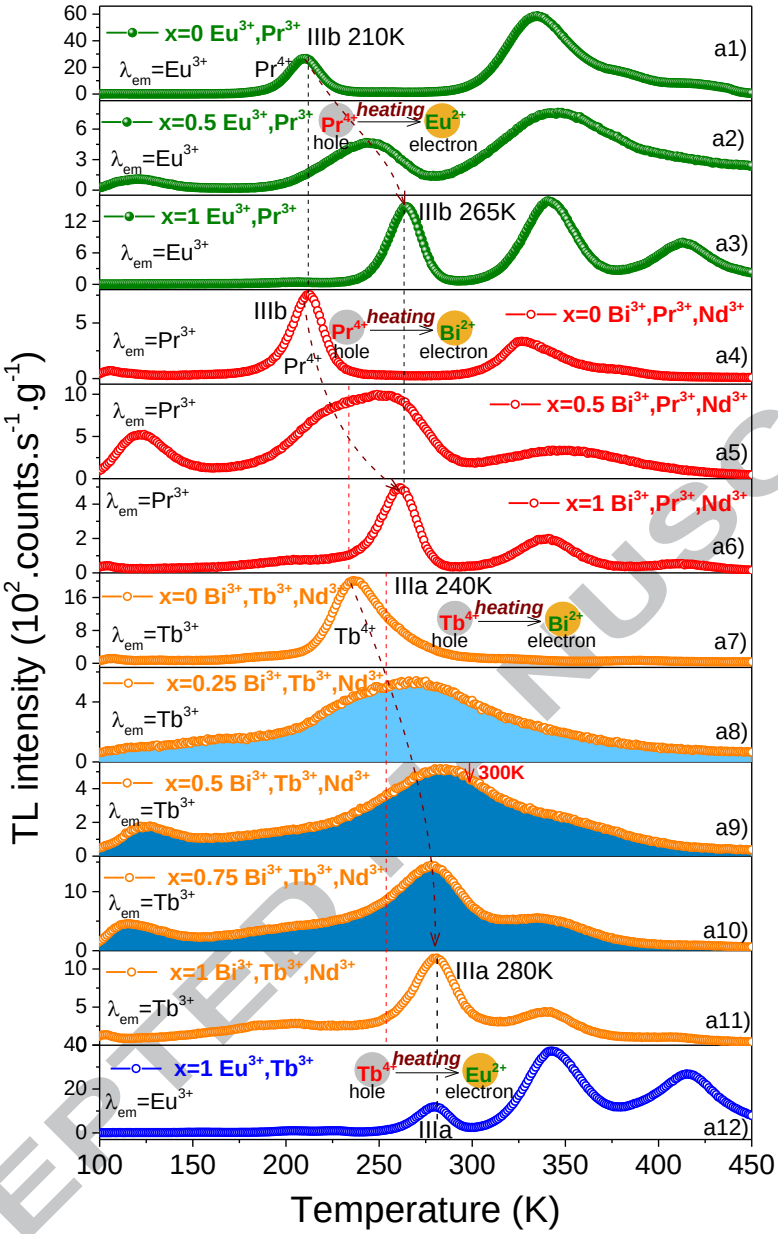


Fig. 11. Low-temperature TL glow curves for $Bi^{3+}$ and/or $Ln^{3+}$ doped $La_{1-x}Gd_xPO_4$ (x=0-1) recorded at a heating of 1 K/s after 600s β irradiation. A 600 nm bandpass filter 600FS40-50 was used to select $Eu^{3+}$ emission in a1)-a3) and a12), and to monitor $Pr^{3+}$ red emission in a4)-a6). A 550 nm bandpass 550FS40-50 was used to monitor $Tb^{3+}$ green emission in a7)-a11).

ACCEPTED MANUSCRIPT

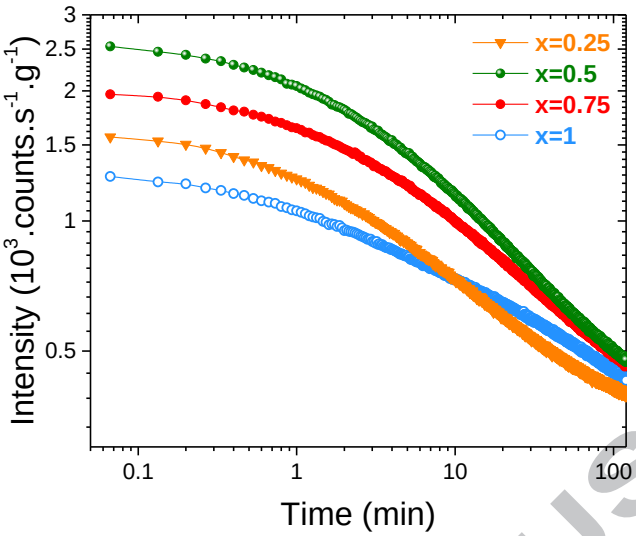


Fig. 12. Room temperature (295 K) isothermal decay curves after β irradiation while monitoring the emission from 400-900 nm for $La_{1-x}Gd_xPO_4$:0.002$Bi^{3+}$,0.005$Tb^{3+}$,0.005$Nd^{3+}$.

Fig. 9b), as another illustrating example, shows the stacked VRBE diagram for $Gd_{1-x}La_xAlO_3$ solid solutions where one can also engineer the hole trap depths of $Tb^{3+}$ and $Pr^{3+}$ by increasing x[49]. By combining $Bi^{3+}$ with $Tb^{3+}$ or $Pr^{3+}$, the holes trapped at $Tb^{4+}$ or $Pr^{4+}$ are predicted to release at a lower temperature than the electrons trapped at $Bi^{2+}$. On recombination with $Bi^{2+}$, $Bi^{3+}$ in its excited state is formed giving $Bi^{3+}$ emission and also $Nd^{3+}$ SWIR luminescence by energy transfer from $Bi^{3+}$ to $Nd^{3+}$. Tuneable thermally stimulated $Nd^{3+}$ SWIR emission is proposed through valence band engineering and using the possible energy transfer from $Bi^{3+}$ to $Nd^{3+}$ because the broad $Bi^{3+}$ emission band at 300-680 in $GdAlO_3$[56] and $LaAlO_3$[21, 57] overlaps with the $Nd^{3+}$ 4f-4f excitation bands like in Fig. 2a). Note that $Bi^{3+}$ can act both as electron and as hole capturing centre like in La-, Y-, and $LuPO_4$[35], one may also engineer the hole release from $Bi^{4+}$ and the recombination with the electrons at $Bi^{2+}$ followed by $Nd^{3+}$ SWIR emission via ET of $Bi^{3+}$→$Nd^{3+}$ in $Bi^{3+}$-$Nd^{3+}$-codoped compounds.

## 5. Conclusions

ACCEPTED MANUSCRIPT

Data from thermoluminescence, fluorescence decay curves, photoluminescence spectroscopy, and ideas from constructed VRBE schemes have been combined to demonstrate the concept of rational design of thermally stimulated $Nd^{3+}$ luminescence between ~900-1700 nm. A new combination of using efficient energy transfer from $Bi^{3+}$ to $Nd^{3+}$ and using an adjustable hole trap depth via valence band engineering is presented in bismuth and lanthanides doped rare earth ortho-phosphate model compounds. We demonstrated that 1.06 μm $Nd^{3+}$ photoluminescence can be realized by efficient energy transfer (ET) from $Bi^{3+}$ to $Nd^{3+}$ rather than by ET from $Tb^{3+}$ to $Nd^{3+}$ in $YPO_4$. The temperature of thermally stimulated $Bi^{3+}$ emission needs then to be designed to further exploit the above energy transfer process from $Bi^{3+}$ to $Nd^{3+}$. By combing ~2.7 eV deep $Bi^{3+}$ electron trap with ~1.42 eV deep hole traps of $Tb^{3+}$, $Pr^{3+}$, or $Bi^{3+}$ in ortho phosphate compounds the holes captured at $Tb^{4+}$, $Pr^{4+}$, or $Bi^{4+}$ liberate at a lower temperature than that of electrons captured at $Bi^{2+}$. On recombination with $Bi^{3+}$, $Bi^{3+}$ in its excited state is formed producing $Bi^{3+}$ A-band emission and also owing to energy transfer from $Bi^{3+}$ to $Nd^{3+}$ the SWIR $Nd^{3+}$ $^4F_{3/2}\rightarrow{}^4I_j$ (j=9/2, 11/2, 13/2) emissions appear in $YPO_4$:0.005$Bi^{3+}$,0.005$Nd^{3+}$ and $YPO_4$:0.005$Bi^{3+}$,0.005$Ln^{3+}$,0.005$Nd^{3+}$ (Ln=Tb and Pr). Here, the thermally stimulated $Nd^{3+}$ SWIR emission is obtained by means of hole release rather than the more commonly reported electron release. We demonstrated that the temperature when thermally stimulated $Nd^{3+}$ 1.06 μm emission appears can be tailored by valence band engineering in $Y_{1-x}Lu_xPO_4$ and $La_{1-x}Gd_xPO_4$, resulting in $Tb^{3+}$ and $Pr^{3+}$ hole trap depth changing. The tailoring was demonstrated for $Y_{1-x}Lu_xPO_4$ and $La_{1-x}Gd_xPO_4$ but can equally well be applied to other compounds like the solid solutions $Gd_{1-x}La_xAlO_3$. Our work shows a new general technique to deep understand afterglow mechanisms and to the rational design of SWIR afterglow phosphors by a new combination of efficient energy transfer from $Bi^{3+}$ to $Nd^{3+}$ and using adjustable hole release processes by valence band engineering. This

ACCEPTED MANUSCRIPT

work also opens the avenue to motivate scientists to explore novel SWIR afterglow phosphors in a design way instead of by trial and error approach.

## 6. Acknowledgements

T. Lyu thanks the financial support from the Chinese Scholarship Council for his PhD research (Tianshuai Lyu: 201608320151). We acknowledge Evert. P. J. Merkx from the Delft University of Technology for supporting the recording of the photoluminescence excitation spectra of $Nd^{3+}$-doped $YPO_4$ crystals using the OPO laser beam.

## Reference

[1] S.W.S. McKeever, Thermoluminescence of Solids, Cambridge University Press, Cambridge, 1985.

[2] R. Chen, S.W. McKeever, Theory of thermoluminescence and related phenomena, World Scientific1997.

[3] A.J.J. Bos, Thermoluminescence as a Research Tool to Investigate Luminescence Mechanisms, Materials 10 (2017) 1357.

[4] Y. Zhang, R. Huang, H. Li, D. Hou, Z. Lin, J. Song, Y. Guo, H. Lin, C. Song, Z. Lin, J. Robertson, Germanium substitution endowing $Cr^{3+}$-doped zinc aluminate phosphors with bright and super-long near-infrared persistent luminescence, Acta Materialia 155 (2018) 214-221.

[5] T. Matsuzawa, Y. Aoki, N. Takeuchi, Y. Murayama, New long phosphorescent phosphor with high brightness, $SrAl_2O_4:Eu^{2+},Dy^{3+}$, Journal of the Electrochemical Society 143 (1996) 2670-2673.

[6] A.J.J. Bos, Theory of thermoluminescence, Radiation Measurements 41 (2006) S45-S56.

[7] J. Xu, S. Tanabe, Persistent luminescence instead of phosphorescence: History, mechanism, and perspective, Journal of Luminescence 205 (2019) 581-620.

[8] Y. Zhuang, Y. Lv, L. Wang, W. Chen, T.-L. Zhou, T. Takeda, N. Hirosaki, R.-J. Xie, Trap Depth Engineering of $SrSi_2O_2N_2:Ln^{2+},Ln^{3+}$ ($Ln^{2+}$ = Yb, Eu; $Ln^{3+}$ = Dy, Ho, Er) Persistent Luminescence Materials for Information Storage Applications, ACS Applied Materials & Interfaces 10 (2018) 1854-1864.

ACCEPTED MANUSCRIPT

[9] Y. Li, M. Gecevicius, J. Qiu, Long persistent phosphors-from fundamentals to applications, Chemical Society Reviews 45 (2016) 2090-2136.

[10] H. Lin, B. Wang, Q. Huang, F. Huang, J. Xu, H. Chen, Z. Lin, J. Wang, T. Hu, Y. Wang, $Lu_2CaMg_2(Si_{1-x}Ge_x)_3O_{12}:Ce^{3+}$ solid-solution phosphors: bandgap engineering for blue-light activated afterglow applicable to AC-LED, Journal of Materials Chemistry C 4 (2016) 10329-10338.

[11] J. Wang, Q. Ma, Y. Wang, H. Shen, Q. Yuan, Recent progress in biomedical applications of persistent luminescence nanoparticles, Nanoscale 9 (2017) 6204-6218.

[12] T. Maldiney, A. Bessière, J. Seguin, E. Teston, S.K. Sharma, B. Viana, A.J.J. Bos, P. Dorenbos, M. Bessodes, D. Gourier, D. Scherman, C. Richard, The in vivo activation of persistent nanophosphors for optical imaging of vascularization, tumours and grafted cells, Nat Mater 13 (2014) 418-426.

[13] A.M. Smith, M.C. Mancini, S. Nie, Second window for in vivo imaging, Nature Nanotechnology 4 (2009) 710.

[14] D. Chen, J. Huang, T.J. Jackson, Vegetation water content estimation for corn and soybeans using spectral indices derived from MODIS near- and short-wave infrared bands, Remote Sensing of Environment 98 (2005) 225-236.

[15] A. Zhang, Z. Sun, M. Jia, G. Liu, F. Lin, Z. Fu, Simultaneous luminescence in Ⅰ, Ⅱ and III biological windows realized by using the energy transfer of $Yb^{3+} \rightarrow Er^{3+}/Ho^{3+} \rightarrow Cr^{3+}$, Chemical Engineering Journal 365 (2019) 400-404.

[16] S. Zhou, N. Jiang, B. Zhu, H. Yang, S. Ye, G. Lakshminarayana, J. Hao, J. Qiu, Multifunctional Bismuth-Doped Nanoporous Silica Glass: From Blue-Green, Orange, Red, and White Light Sources to Ultra-Broadband Infrared Amplifiers, Advanced Functional Materials 18 (2008) 1407-1413.

[17] G. Hong, J.T. Robinson, Y. Zhang, S. Diao, A.L. Antaris, Q. Wang, H. Dai, In Vivo Fluorescence Imaging with $Ag_2S$ Quantum Dots in the Second Near‐Infrared Region, Angewandte Chemie 124 (2012) 9956-9959.

ACCEPTED MANUSCRIPT

[18] W. Fan, N. Lu, C. Xu, Y. Liu, J. Lin, S. Wang, Z. Shen, Z. Yang, J. Qu, T. Wang, S. Chen, P. Huang, X. Chen, Enhanced Afterglow Performance of Persistent Luminescence Implants for Efficient Repeatable Photodynamic Therapy, ACS Nano 11 (2017) 5864-5872.

[19] J. Xu, D. Murata, Y. Katayama, J. Ueda, S. Tanabe, $Cr^{3+}$/$Er^{3+}$ co-doped $LaAlO_3$ perovskite phosphor: a near-infrared persistent luminescence probe covering the first and third biological windows, Journal of Materials Chemistry B 5 (2017) 6385-6393.

[20] F. Liu, Y. Liang, Y. Chen, Z. Pan, Divalent Nickel-Activated Gallate-Based Persistent Phosphors in the Short-Wave Infrared, Advanced Optical Materials 4 (2016) 562-566.

[21] R.H.P. Awater, P. Dorenbos, The $Bi^{3+}$ 6s and 6p electron binding energies in relation to the chemical environment of inorganic compounds, Journal of Luminescence 184 (2017) 221-231.

[22] P. Dorenbos, A Review on How Lanthanide Impurity Levels Change with Chemistry and Structure of Inorganic Compounds, ECS Journal of Solid State Science and Technology 2 (2013) R3001-R3011.

[23] P. Dorenbos, Modeling the chemical shift of lanthanide 4f electron binding energies, Physical Review B 85 (2012) 165107.

[24] J. Ueda, S. Miyano, S. Tanabe, Formation of Deep Electron Traps by $Yb^{3+}$ Codoping Leads to Super-Long Persistent Luminescence in $Ce^{3+}$-Doped Yttrium Aluminum Gallium Garnet Phosphors, ACS Applied Materials & Interfaces 10 (2018) 20652-20660.

[25] Z. Pan, Y.-Y. Lu, F. Liu, Sunlight-activated long-persistent luminescence in the near-infrared from $Cr^{3+}$-doped zinc gallogermanates, Nat Mater 11 (2012) 58-63.

[26] F. Liu, W. Yan, Y.-J. Chuang, Z. Zhen, J. Xie, Z. Pan, Photostimulated near-infrared persistent luminescence as a new optical read-out from $Cr^{3+}$-doped $LiGa_5O_8$, Scientific Reports 3 (2013) 1554.

[27] Y. Li, S. Zhou, Y. Li, K. Sharafudeen, Z. Ma, G. Dong, M. Peng, J. Qiu, Long persistent and photo-stimulated luminescence in $Cr^{3+}$-doped Zn-Ga-Sn-O phosphors for deep and reproducible tissue imaging, Journal of Materials Chemistry C 2 (2014) 2657-2663.

ACCEPTED MANUSCRIPT

[28] Y.-J. Liang, F. Liu, Y.-F. Chen, X.-J. Wang, K.-N. Sun, Z. Pan, New function of the $Yb^{3+}$ ion as an efficient emitter of persistent luminescence in the short-wave infrared, Light Sci Appl. 5 (2016) e16124.

[29] N. Yu, F. Liu, X. Li, Z. Pan, Near infrared long-persistent phosphorescence in $SrAl_2O_4:Eu^{2+},Dy^{3+},Er^{3+}$ phosphors based on persistent energy transfer, Applied Physics Letters 95 (2009) 231110.

[30] J. Xu, D. Murata, J. Ueda, S. Tanabe, Near-infrared long persistent luminescence of $Er^{3+}$ in garnet for the third bio-imaging window, Journal of Materials Chemistry C 4 (2016) 11096-11103.

[31] Y. Liang, F. Liu, Y. Chen, X. Wang, K. Sun, Z. Pan, Extending the applications for lanthanide ions: efficient emitters in short-wave infrared persistent luminescence, Journal of Materials Chemistry C 5 (2017) 6488-6492.

[32] Y. Liang, F. Liu, Y. Chen, X. Wang, K. Sun, Z. Pan, Red/near-infrared/short-wave infrared multi-band persistent luminescence in $Pr^{3+}$-doped persistent phosphors, Dalton Transactions 46 (2017) 11149-11153.

[33] J. Xu, S. Tanabe, A.D. Sontakke, J. Ueda, Near-infrared multi-wavelengths long persistent luminescence of $Nd^{3+}$ ion through persistent energy transfer in $Ce^{3+}$, $Cr^{3+}$ co-doped $Y_3Al_2Ga_3O_{12}$ for the first and second bio-imaging windows, Applied Physics Letters 107 (2015) 081903.

[34] T. Lyu, P. Dorenbos, Charge carrier trapping processes in lanthanide doped $LaPO_4$, $GdPO_4$, $YPO_4$, and $LuPO_4$, Journal of Materials Chemistry C 6 (2018) 369-379.

[35] T. Lyu, P. Dorenbos, $Bi^{3+}$ acting both as an electron and as a hole trap in La-, Y-, and $LuPO_4$, Journal of Materials Chemistry C 6 (2018) 6240-6249.

[36] F. You, A.J.J. Bos, Q. Shi, S. Huang, P. Dorenbos, Thermoluminescence investigation of donor ($Ce^{3+}$, $Pr^{3+}$, $Tb^{3+}$) acceptor ($Eu^{3+}$, $Yb^{3+}$) pairs in $Y_3Al_5O_{12}$, Physical Review B 85 (2012) 115101.

[37] R.H.P. Awater, L.C. Niemeijer-Berghuijs, P. Dorenbos, Luminescence and charge carrier trapping in $YPO_4$:Bi, Optical Materials 66 (2017) 351-355.

[38] P. Dorenbos, Charge transfer bands in optical materials and related defect level location, Optical Materials 69 (2017) 8-22.

ACCEPTED MANUSCRIPT

[39] D.L. Dexter, J.H. Schulman, Theory of Concentration Quenching in Inorganic Phosphors, The Journal of Chemical Physics 22 (1954) 1063-1070.

[40] M. Jiao, Y. Jia, W. Lu, W. Lv, Q. Zhao, B. Shao, H. You, $Sr_3GdNa(PO_4)_3F:Eu^{2+},Mn^{2+}$: a potential color tunable phosphor for white LEDs, Journal of Materials Chemistry C 2 (2014) 90-97.

[41] A.J.J. Bos, P. Dorenbos, A. Bessière, A. Lecointre, M. Bedu, M. Bettinelli, F. Piccinelli, Study of TL glow curves of $YPO_4$ double doped with lanthanide ions, Radiation Measurements 46 (2011) 1410-1416.

[42] M. Puchalska, P. Bilski, GlowFit—a new tool for thermoluminescence glow-curve deconvolution, Radiation Measurements 41 (2006) 659-664.

[43] J. Azorín, Determination of thermoluminescence parameters from glow curves—I. A review, International Journal of Radiation Applications and Instrumentation. Part D. Nuclear Tracks and Radiation Measurements 11 (1986) 159-166.

[44] W. Hoogenstraaten, Electron traps in zinc–sulphide phosphors, Philips Res. Rep 13 (1958) 515–693.

[45] R. Chen, S.A.A. Winer, Effects of Various Heating Rates on Glow Curves, Journal of Applied Physics 41 (1970) 5227-5232.

[46] A.J.J. Bos, P. Dorenbos, A. Bessière, B. Viana, Lanthanide energy levels in $YPO_4$, Radiation Measurements 43 (2008) 222-226.

[47] W. Jean-François, M. Ali, T.-B. Wan-Ü Lydia, C. Norbert, L. Omar, S. Nissan, S. Jack, Analysis of the free ion $Nd^{3+}$ spectrum (Nd IV), Journal of Physics B: Atomic, Molecular and Optical Physics 40 (2007) 3957-3972.

[48] T. Hoshina, S. Kuboniwa, 4f-5d Transition of $Tb^{3+}$ and $Ce^{3+}$ in $MPO_4$ (M=Sc, Y and Lu), Journal of the Physical Society of Japan 31 (1971) 828-840.

[49] H. Luo, A.J.J. Bos, P. Dorenbos, Controlled Electron–Hole Trapping and Detrapping Process in $GdAlO_3$ by Valence Band Engineering, The Journal of Physical Chemistry C 120 (2016) 5916-5925.

ACCEPTED MANUSCRIPT

[50] R.H.P. Awater, P. Dorenbos, Towards a general concentration quenching model of $Bi^{3+}$ luminescence, Journal of Luminescence 188 (2017) 487-489.

[51] A. Mraouefel, L. Guerbous, A. Boukerika, M. Diaf, A. Mendoud, M. Seraiche, M. Taibeche, M.S.E. Hamroun, N. Baadji, Effect of the vanadium concentration on structural and photoluminescence of $YP_{1-x}V_xO_4$: 1 at. % $Tb^{3+}$ nanophosphors, Optical Materials 65 (2017) 129-136.

[52] A. Lecointre, A. Bessière, A.J.J. Bos, P. Dorenbos, B. Viana, S. Jacquart, Designing a Red Persistent Luminescence Phosphor: The Example of $YPO_4:Pr^{3+},Ln^{3+}$ (Ln = Nd, Er, Ho, Dy), The Journal of Physical Chemistry C 115 (2011) 4217-4227.

[53] P.W. Tasker, A.M. Stoneham, An appraisal of the molecular model for the Vk centre, Journal of Physics and Chemistry of Solids 38 (1977) 1185-1189.

[54] R. Gazzinelli, G.M. Ribeiro, M.L. de Siqueira, ESR and endor studies of the VK center in $SrF_2$, Solid State Communications 13 (1973) 1131-1134.

[55] N.F. Mott, A.M. Stoneham, The lifetime of electrons, holes and excitons before self-trapping, Journal of Physics C: Solid State Physics 10 (1977) 3391.

[56] A.M. Srivastava, H.A. Comanzo, The ultraviolet and visible luminescence of $Bi^{3+}$ in the orthorhombic perovskite, $GdAlO_3$, Optical Materials 63 (2017) 118-121.

[57] L.I. van Steensel, S.G. Bokhove, A.M. van de Craats, J. de Blank, G. Blasse, The luminescence of $Bi^{3+}$ in $LaInO_3$ and some other perovskites, Materials Research Bulletin 30 (1995) 1359-1362.

ACCEPTED MANUSCRIPT

ACCEPTED MANUSCRIPT

## Graphical abstract

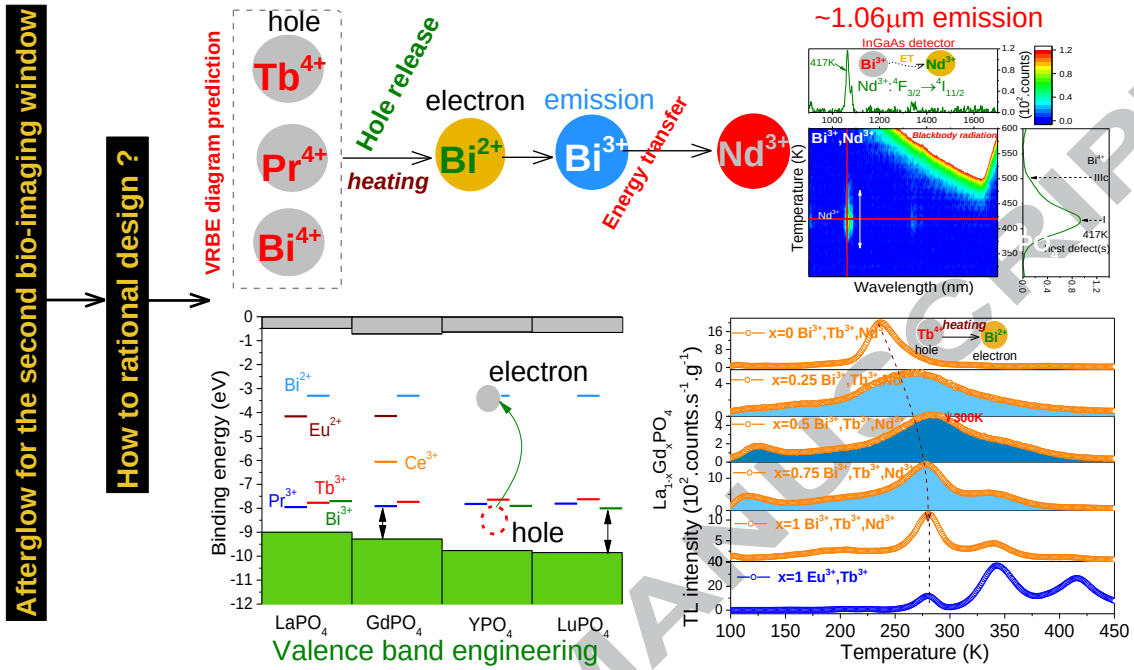


A general methodology to the rational design of thermally stimulated short-wave infrared (SWIR) luminescence between ~900 and 1700 nm is achieved by a new combination of using efficient energy transfer from $Bi^{3+}$ to $Nd^{3+}$ and an adjustable hole trap depth via valence band engineering.

ACCEPTED MANUSCRIPT

**Highlights**

- A general methodology to rationally design infrared afterglow between ~900-1700nm
- New combination of energy transfer of $Bi^{3+} \rightarrow Nd^{3+}$ and adjustable hole trap depth
- $Bi^{3+}$ as deep electron trap and recombination luminescence centre
- Our work shows a new general technique to deep understand afterglow mechanisms
- Explore afterglow phosphor in a design way instead of by trial-and-error approach

ACCEPTED MANUSCRIPT